ACADEMIA ROMÂNĂ
Revue Roumaine de Chimie
https://www.icf.ro/rrch/

Rev. Roum. Chim.,
2024, *69*(1–2), 83–96
DOI: 10.33224/rrch.2024.69.1-2.10

SPECTRAL CHARACTERIZATION AND ANTIBACTERIAL, ANTIFUNGAL, ANTIVIRAL ACTIVITY OF SALICYL BASED NEW SCHIFF BASES AND THEIR Co(II), Ni(II), Cu(II), Zn(II), AND Pd(II) COMPLEXES**

Dildora PARDAEVA,[a] Aydin TAVMAN,[b,*] Demet GÜRBÜZ,[b] Mayram HACIOGLU,[c] Fatıma Nur YILMAZ,[c] Onur ŞAHIN,[d] A. Seher BIRTEKSÖZ TAN[c] and Adem ÇINARLI[b]

[a]Istanbul University-Cerrahpasa, Institute of Graduate Education, Department of Chemistry, 34320, Avcilar, Istanbul, Turkey
[b]Istanbul University-Cerrahpaşa, Faculty of Engineering, Department of Chemistry, 34320, Avcilar, Istanbul, Turkey
[c]Istanbul University, Faculty of Pharmacy, Department of Pharmaceutical Microbiology, 34452, Beyazit, Istanbul, Turkey
[d]Sinop University, Department of Occupational Health and Safety, Faculty of Health Sciences, 57000 Sinop, Turkey

Received November 6, 2023

Two new salicyl based Schiff bases derived from 3,5-dichlorosalicylaldehyde and 4-(chloro/*tert*-butyl)-2-aminophenols (**H_2L^1** and **H_2L^2**) and their complexes with cobalt(II), nickel(II), copper(II), zinc(II), and palladium(II), {[M(**L^n**)(H_2O)]·xH_2O, M(II) = Co(II) (*n* = 1, 2; *x* = 1), Ni(II) (*n* = 1, *x* = 2; *n* = 2, *x* = 0), Cu(II) (*n* = 1, 2; *x* = 0), Zn(II) (*n* = 1, 2; *x* = 0); K[Pd(**L^n**)Cl]; *n* = 1, 2}, were synthesized and characterized. The structural characteristics of the complexes were examined by means of elemental analysis, molar conductivity, magnetic moment, thermogravimetric analysis (TGA), UV-visible, FT-IR, and NMR spectroscopy. In addition, the crystal structures of **H_2L^1** and **H_2L^2** were determined by X-ray single diffraction measurements. All the complexes are non-electrolyte with 1:1 M:L ratio. Antibacterial and antifungal activity of the compounds was evaluated against six bacteria and three fungi. In general, all the compounds showed moderate antimicrobial activity. Some of the complexes exhibited higher activity towards some microorganisms than the ligands. Antiviral activity of the compounds was tested against Parainfluenza Type-2 virus. The fact that **H_2L^2** has a higher antiviral effect than **H_2L^1** can be evaluated as that the *tert*-butyl group promotes the antiviral effect.

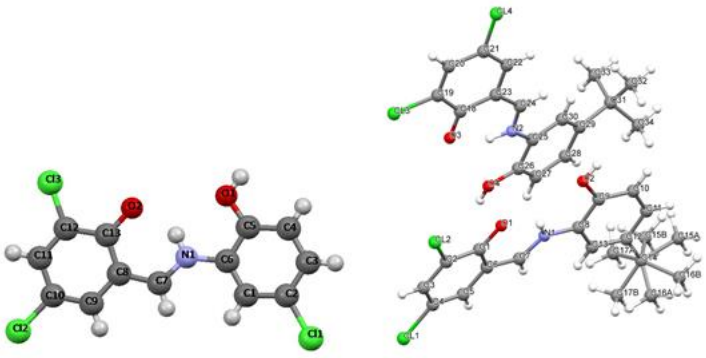

INTRODUCTION

Schiff bases or imines with the other name are a research topic of high interest, especially in the fields of chemistry and health, due to their wide range of application possibilities. For instance, they have many effects and properties in the field of human health such as antibacterial, antiviral,

* Corresponding author: atavman@iuc.edu.tr
** Supplementary Information on https://www.icf.ro/rrch/ or https://revroum.lew.ro

antifungal, anti-inflammatory, analgesic, anticonvulsant, antituberculosis, anticancer, antioxidant, antihelmintic, antimalarial and anti-HIV.[1–5]

Furthermore, Schiff bases are a highly preferred group of compounds as ligands in coordination chemistry due to their high donor properties and being chelating agents.[6–8] Complexes of some transition metal ions and Schiff bases are known to have various applications in areas such as homogeneous or heterogeneous catalysis,[9,10] analytical reagents,[11] dyeing of textile fabrics[12,13] etc. Innumerable Schiff bases and their some metal complexes, especially those with the first row transition metal ions, have been investigated for their important and interesting characteristics, such as the removal of some toxic metal ions due to their complex forming capacity, photochromic properties and reversible oxygen binding ability.[14,15]

Schiff bases derived from o-aminophenols and salicylaldehydes are a class of compounds of high interest because of their forming chelate structures and variety of uses and interesting properties.[16] The simplest example of this class compound is "2-{[(2-hydroxyphenyl)imino]methyl}phenol". Their complexation effects are particularly high and they are forming strong chelate complexes exhibiting tridentate characteristic.[17] There are studies on the antimicrobial activities of Schiff bases and various metal complexes derived from many salicyl aldehyde derivatives. For instance, anticancer activity of the Schiff base organotin(IV) compounds based on salicylaldehyde-*o*-aminophenol were reported.[18] The antimicrobial activities of some metal complexes of the ONO Schiff base compound were examined and it was determined that Mn(II), Cu(II) and Co(II) complexes showed significant activity.[19] Schiff base 3-methoxy-N-salicylidene-*o*-amino phenol complexes with some transition metal ions and their antibacterial, antifungal activities were investigated by Abo-Aly *et al.*[20] Antibacterial activity of mixed ligands of Schiff base and it's metal(II) complexes derived from ampicilin, 3-aminophenol and benzaldehyde was studied.[21] In many of our studies, the antimicrobial activities of such Schiff bases and complexes have been examined, and it was determined that many Schiff bases and their complexes showed significant antibacterial and antifungal activity.[7,8,16,17a] As is known, Cu(II) and Zn(II) ions have important roles in the human body. Cobalt, which is a part of vitamin B12, is also an essential metal. Some Ni(II) and Pd(II) complexes have also been reported to have various biological activities.[22,23] In this study, two new salicyl based Schiff bases 2-hydroxyphenyl)imino]methyl}phenol derivatives) (**H_2L^1** and **H_2L^2**, Fig. 1) and their complexes with Co(II), Ni(II), Cu(II), Zn(II) and Pd(II) were prepared and characterized. In addition, antibacterial, antifungal and antiviral activities of the compounds were tested towards six bacteria, three fungi and Parainfluenza Type-2 virus. The structural characteristics and antimicrobial activity of the ligands and the complexes were evaluated. The aim of the study is to obtain new Schiff bases and complexes, examine their structural characteristics, reveal their antibacterial and antiviral properties, and contribute to the literature in this field.

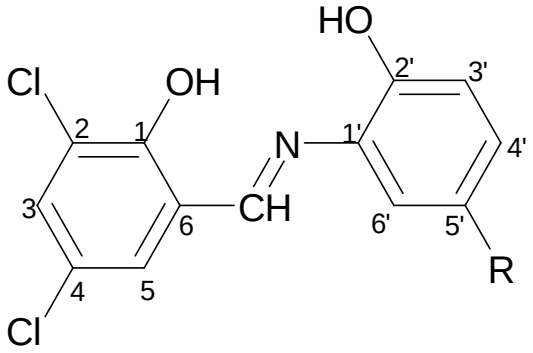

R = Cl (**H_2L^1**), R = $C(CH_3)_3$ (**H_2L^2**)

Fig. 1 – Chemical structure of the Schiff bases in the study

RESULTS AND DISCUSSION

Crystal structures of H_2L^1 and H_2L^2

Crystal data and structure refinement parameters related **H_2L^1** and **H_2L^2** are given in Table 1. Some important bond distances and bond angles are presented in Table S1, hydrogen bond parameters in Table S2. Molecular structures of **H_2L^1** and **H_2L^2** are shown in Figs. 2 and 3, respectively, and the molecular planes and intermolecular hydrogen bonds in Figs. S1 and S2, respectively.

From the X-ray data, it appears that the keto structure is valid on both Schiff bases (Figs. 2 and 3) in solid state. However, the crystal systems of **H_2L^1** and **H_2L^2** are different, namely orthorombic and monoclinic, respectively. In the crystal structure of both ligands, the C–O bond length in

the 4,6-dichlorophenol part is shorter than the other (hydroxyphenylimino part) {1.284(6) and 1.341(6) for H_2L^1; 1.271(6) and 1.352(6) Å for H_2L^2, respectively}. This difference between the C–O bond lengths is due to the keto structure being more dominant than the enol structure. Accordingly, the solid state structure of H_2L^1 is as in Fig. 4.

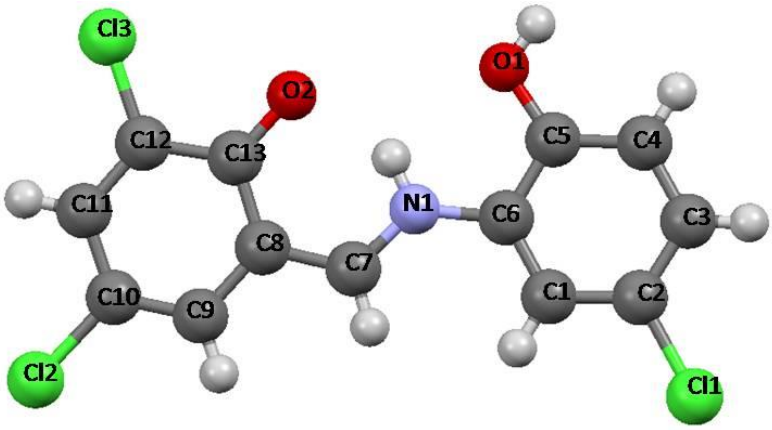

Fig. 2 – Molecular structure of H_2L^1 showing the atom numbering scheme.

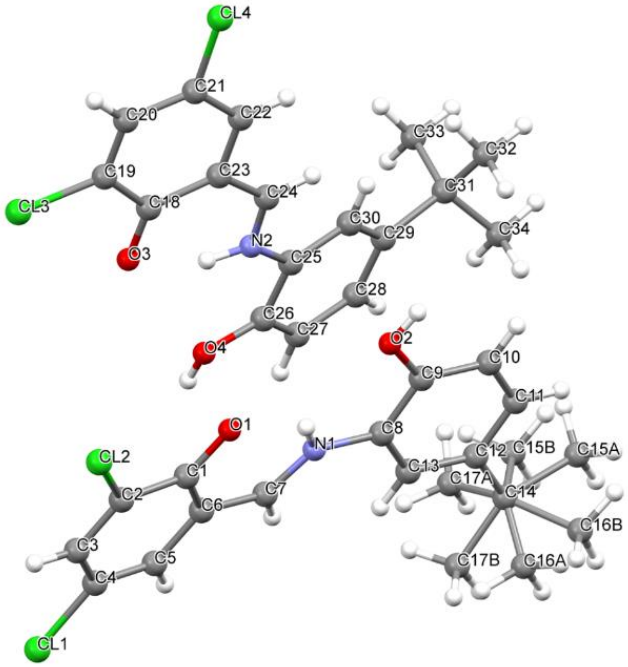

Fig. 3 – Molecular structure of H_2L^2 showing the atom numbering scheme.

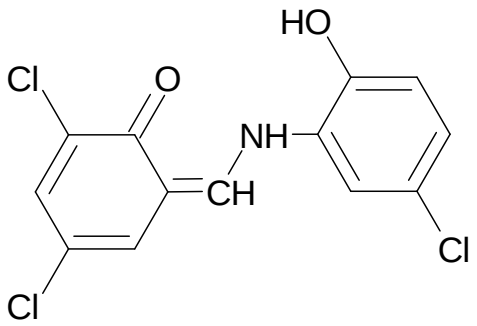

Fig. 4 – Keto structure of H_2L^1.

Table 1

Crystal data and structure refinement parameters

Crystal data	H_2L^1	H_2L^2
Empirical formula	$C_{13}H_8Cl_3NO_2$	$C_{17}H_{17}Cl_2NO_2$
Formula weight	316.55	338.21
Temperature, (K)	296	296
Crystal system	Orthorhombic	Monoclinic
Color	Orange	Orange
Space group	*Pbca*	$P2_1/c$
a (Å)	14.5718 (15)	15.212 (3)
b (Å)	6.2285 (5)	22.032 (5)
c (Å)	28.615 (3)	9.9638 (19)
β (º)	90.00	94.415 (6)
V (Å^3)	2597.1 (4)	3329.4 (12)
Z	8	8
D_c (g cm^{-3})	1.619	1.349
μ (mm^{-1})	0.70	0.40
θ range (º)	2.8-27.7	2.5-26.9
Measured refls.	21490	107364
Independent refls.	2412	6179
R_{int}	0.131	0.072
S	1.06	1.16
R1/wR2	0.071/0.129	0.094/0.192
$\Delta\rho_{max}/\Delta\rho_{min}$ (eÅ^{-3})	0.35/-0.42	0.66/-0.36
CCDC	2194774	2194769

Mass spectra

ESI-MS results support the formation of ligands. **H_2L^1** mol peak was detected as 12.1% and **H_2L^2** mol peak was detected at 60.9% (Fig. S3). The *m*/*z* 278.9 peak seen at 100% abundance in the **H_2L^1** MS spectrum corresponds to the removal of one chlorine and two hydrogen atoms from the molecule (M-Cl-2H) (Fig. S4). No significant results were obtained from ESI-MS analysis for complex compounds (mole peaks of the complexes could not be detected).

Characterization of the complexes

In this study, ten related transition metal complexes were obtained by allowing the ligands (**H_2L^1** and **H_2L^2**) to react with cobalt(II), nickel(II), copper(II), zinc(II) perchlorates and potassium tetrachloropalladat(II) at a molar ratio of 1:1 (Studies conducted with a 1:2 ratio gave the same result, that is, a 1:1 M:L ratio). The ligands are tridentate and have dibasic chelating characteristics.

The M:L ratio was found to be 1:1 in all the complexes. According to the molar conductivity measurements, which range from 1.2 to 33.0 $\Omega^{-1}cm^2mol^{-1}$, all of the complex compounds are non-electrolyte in DMF.[24] The ligands gave immediately khaki green colored precipitates with $Cu(ClO_4)_2$. They showed also similar behavior towards K_2PdCl_4. Cobalt(II), nickel(II) and zinc(II) perchlorates showed different behavior towards to the ligands differently from these two metals under reaction conditions, they did not form the complexes. Therefore, in order to obtain the cobalt(II), nickel(II) and zinc(II) complexes, the pH value of the media was adjusted to around 5 using 5% ethanolic NaOH solution.

Magnetic moment values for [Cu(**L^1**)(H_2O)] and [Cu(**L^2**)(H_2O)] were found to be 1.22 and 1.11 BM, respectively. This may indicates that there is an M-M interaction in the copper(II) complexes. It can be said that the complex may have a dimeric structure and as a result, there is an antiferromagnetic interaction between Cu(II)-Cu(II) ions, causing the magnetic moment value to be lower than expected.[25] Considering that the ligands are tridentate, it is possible to suggest that the complexes have a five-coordination structure bridged over water molecules.[26]

Magnetic moments of [Co(**L^1**)(H_2O)]·H_2O and [Co(**L^2**)(H_2O)]·H_2O complexes were found as 1.42 and 1.54 BM, respectively. This values can be considered as evidence that the four coordinated d^7 complexes is in a low spin state with a square planar geometry of the central ion although slightly lower than expected.[27] The nickel(II) complexes have 2.33 and 2.26 BM magnetic moment values for **H_2L^1** and **H_2L^2**, respectively. These values, which are lower than the expected value for an octahedral or tetrahedral d^8 ion (which is 2.83 BM for two unpaired electrons), can be considered to result from a distorted geometry between tetrahedral and square planar systems, called quasi-tetrahedral.[28]

Infrared spectroscopy

IR spectroscopy data of the obtained compounds are presented in Experimental section. FTIR spectra of the ligands and the complexes are given as supporting information (Figs. S5 and S6). In addition, FTIR spectra of **H_2L^1** and its complexes are presented in Fig. 5 for comparison.

The relatively strong bands appear at 1206 and 1217 cm^{-1} can be assigned to the phenolic C–O group stretching vibrations for $\mathbf{H_2L^1}$ and $\mathbf{H_2L^2}$, respectively. The typical medium band appearing at 2957 cm^{-1} in $\mathbf{H_2L^2}$ is due to the CH bonds of the tertiary butyl group (Fig. S6). Surprisingly, although the keto group was detected in the crystal structure of both ligands, no evidence of the keto group was found in the IR spectra, and bands that could be considered as corresponding to the azomethine HC=N bond were detected at 1626 and 1635 cm^{-1} for $\mathbf{H_2L^1}$ and $\mathbf{H_2L^2}$, respectively.[20] There is probably a balance between the two forms. The medium bands appearing in the range of 1602 and 1611 cm^{-1} in the ligands may be due to stretching vibrations of aromatic C=C bonds.[7,8] By comparing the IR spectra of $\mathbf{H_2L^1}$ and $\mathbf{H_2L^2}$ and their complexes, the IR spectral changes that occur with the complexation were determined. One of the most important changes in the IR spectra is the disappearance of the stretching vibrations of phenolic OH groups at 3200 cm^{-1} in the ligand's spectra with the complexation giving broad bands resulting from intramolecular hydrogen bonding. In addition, there have been significant changes such as shifting at lower wavenumbers and reduction in band intensity, along with the complexation in the medium bands, which occur in the range of 1654 and 1575 cm^{-1} due to the stretching vibrations of the azomethine HC=N and aromatic C=C bonds.

It can be said that the new medium bands appearing in the complexes in the range of 620 – 670 cm^{-1} are due to the coordination of the nitrogen atom of azomethine group. Again, the changes such as shifts and decreases in intensity of the phenolic C–O is one of the most important findings showing the phenolic group deprotonation and oxygen atom coordination. The broad bands between 3200 – 2600 cm^{-1} in $\mathbf{H_2L^1}$ (4-chloro derivative) arise from intramolecular and intermolecular H-bondings. The different appearance of the other ligand ($\mathbf{H_2L^2}$) having a tertiary butyl group should be related to the weaker intermolecular hydrogen bonding according to $\mathbf{H_2L^1}$ (Fig. S6). It is clearly seen that these bands disappear with the formation of the complex, especially in the Pd(II) complexes, that is, with the phenolic oxygen coordination. The bands belonging to uncoordinated water molecules in Co(II) and Ni(II) complexes are clearly visible around 3500 cm^{-1} as broad bands.[29] Although coordinated water molecules in Zn(II) and Cu(II) complexes are weak, they can be detected around 3200 cm^{-1}.[30] The absence of any significant bands other than weak aromatic CH bands above 3000 cm^{-1} in the Pd(II) complexes shows that there is no OH group and water molecules in these complexes (Figs. 5 and S6). When this situation is evaluated together with elemental analysis data, it is possible to claim that the Pd(II) complexes have the K[Pd(**L**)Cl] composition.

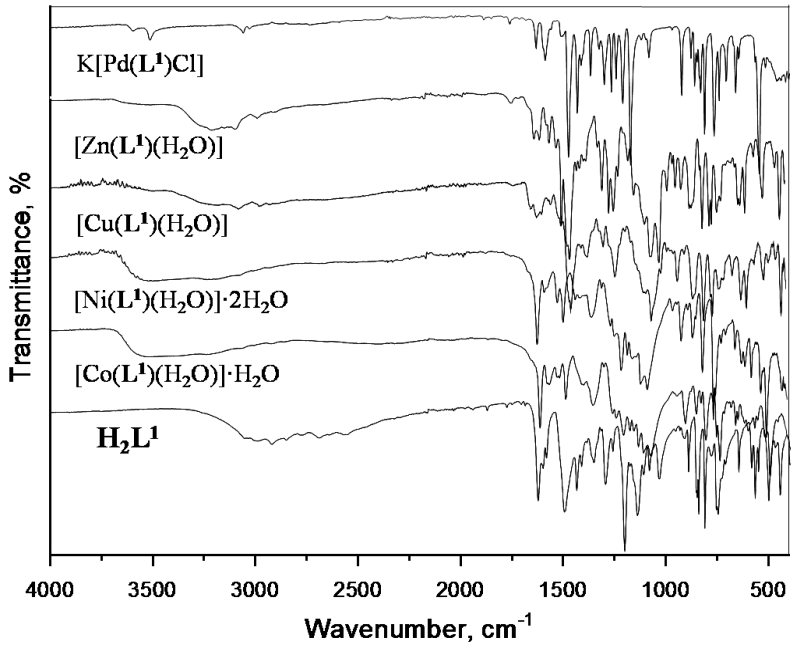

Fig. 5 – FTIR spectra of $\mathbf{H_2L^1}$ and its complexes.

NMR spectroscopy

NMR spectroscopy data of the ligands and Zn(II) and Pd(II) complexes are given in Experimental section. Also ^{1}H- and ^{13}C-NMR spectra of the compounds are given as supporting information (Figs. S7 – S18). In the ^{1}H-NMR spectra of the ligands, one of the phenolic OH protons (OH1, salicyl OH) could not be detected, possibly due to dissociation, while the signal of the other appeared at 10.40 and 10.01 ppm for $\mathbf{H_2L^1}$ and $\mathbf{H_2L^2}$, respectively. The imino hydrogen (–CH=N–) was observed at 9.09 and 9.15 ppm (for $\mathbf{H_2L^1}$ and $\mathbf{H_2L^2}$). As a result of the formation of 1:1 and neutral complexes, OH protons were not detected in the palladium(II) and zinc(II) complexes, while the proton of –CH=N– group shifted to a lower ppm value (upfield shift): It was detected at 8.76 and 8.77 ppm as singlet in the palladium(II) complexes of $\mathbf{H_2L^1}$ and $\mathbf{H_2L^2}$, respectively (Figs. S13 and S17). They were detected at 8.97 and 8.94 ppm for [Zn($\mathbf{L^1}$)(H_2O)] and [Zn($\mathbf{L^2}$)(H_2O)], respectively (Figs. S11 and S15). These changes clearly show that the imine nitrogen is coordinated to the metal ion. The ^{1}H-NMR spectra of $\mathbf{H_2L^1}$ and its Zn(II) complex are comparatively shown in Fig. 6.

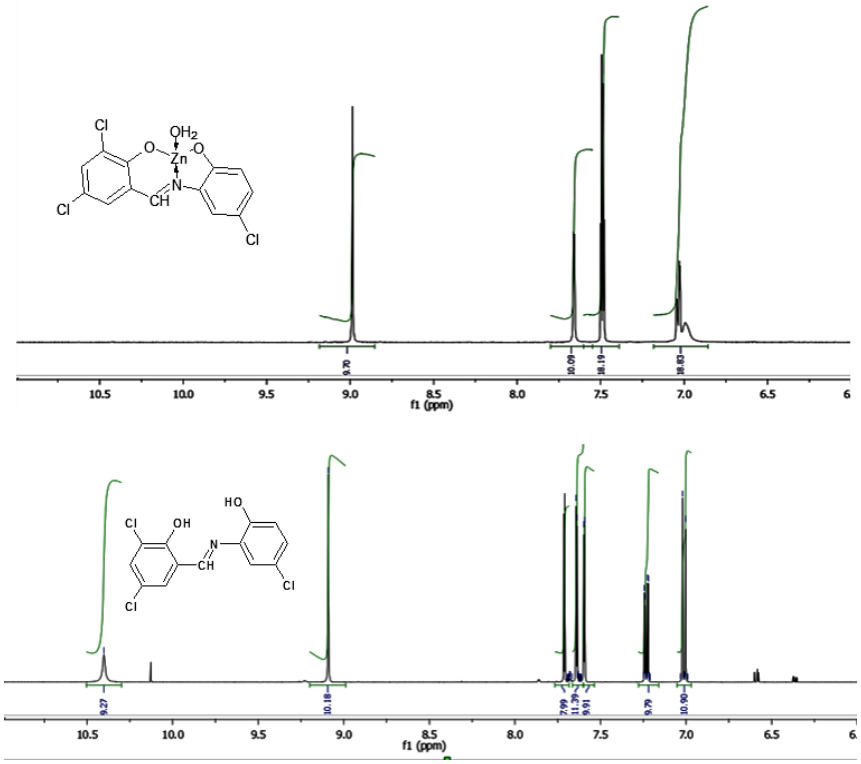

Fig. 6 – ^{1}H-NMR spectra of $\mathbf{H_2L^1}$ and its Zn(II) complex, [Zn($\mathbf{L^1}$)H_2O], in DMSO-d_6.

Similarly, in the ^{13}C-NMR spectra of the Zn(II) and Pd(II) complexes (Figs. S12, S14, S16 and S18) it is seen that the carbon atoms most affected by the complex formation are the carbon atoms attached to the OH groups and the imine carbon atom (–CH=N–). The imine carbon atoms are detected at 161.1 ppm in $\mathbf{H_2L^1}$ and at 167.2 and 164.1 ppm in its palladium(II) and zinc(II) complexes, respectively (downfield shift). The C1–OH and The C2'–OH carbon atoms of $\mathbf{H_2L^1}$ appeared at 158.3 and 150.6 ppm, respectively, and shifted to 163.8 and 153.7 ppm, respectively, in the zinc(II) complex. These carbon atoms were detected at 156.8 and 147.3 ppm in the Pd(II) complex.

Thermogravimetric studies

The major features of the thermal analysis of the complexes are given in Experimental section. The thermal analysis curves of the $\mathbf{H_2L^1}$ complexes are shown in Fig. 7 (The thermal analysis curves of the $\mathbf{H_2L^2}$ complexes are given in Supporting information, Fig. S19). The samples of the complexes were heated from room temperature up

to 500 ºC in air atmosphere. It was observed that the thermal degradation of the complexes occurred at four stages in the most of the complexes. At the first stage, uncoordinated lattice water was lost through elimination from 40 to 100 ºC. At the second stage, coordinated water molecules are removed above 100 ºC. A mass loss of 8.5% was observed in the TGA curve of [Ni(**L**^{1})(H_2O)]·2H_2O below 100 °C corresponds to two moles of lattice water. A mass loss of 3.6 – 5.0% below 100 °C in both cobalt complexes indicates that there is one mole of lattice water in each of these complexes. Considering the mass loss between 3.6 – 5.0% in the 150 – 200 °C range in the TGA curve of Co(II), Ni(II), Cu(II) and Zn(II) complexes, it is possible to suggest that one mole of water molecules is coordinated in these complexes. In addition, it is possible to say that both Pd(II) complexes have neither lattice nor coordinated water molecules.

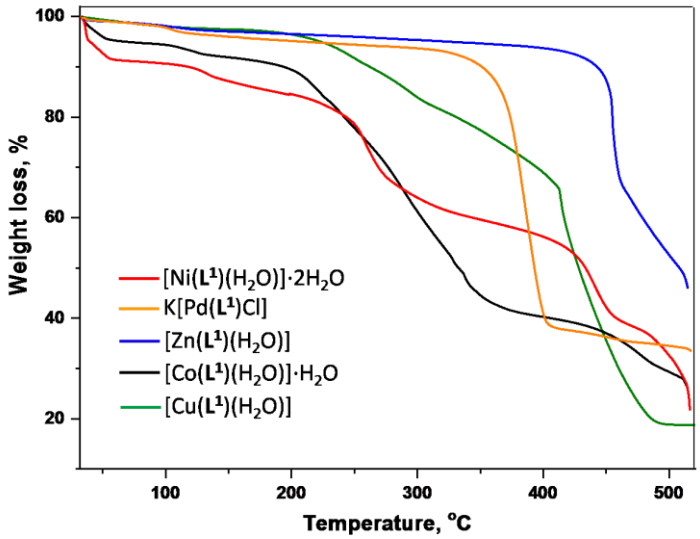

Fig. 7 – TGA curves of **H$_2$L^1** complexes in the study

While the Ni(II), Cu(II) and Co(II) complexes of **H$_2$L^1** begin to decompose above 200 °C, it is observed that the Pd(II) and Zn(II) complexes start to decompose after 370 and 450 °C, respectively. Considering the mass loss rates, the approximately 20% mass loss detected in Ni(II), Zn(II) and Cu(II) complexes at different temperatures is similar. This mass loss corresponds to two chlorine atoms per molecule. In the Pd(II) and Co(II) complexes, a 60% mass loss is observed around 400 °C, which indicates that there is a different degradation mechanism in these complexes. It is observed that all complexes completely decompose above 550 °C and turn into metal oxide forms.

There is a different thermal behavior in the **H$_2$L^2** complexes, and this is due to the structure of the ligand. The fact that **H$_2$L^2** melts at lower temperature than **H$_2$L^2** (**H$_2$L^1**: 263 °C, **H$_2$L^2**: 238 °C) causes the complexes of **H$_2$L^2** to begin to decompose at lower temperatures according to the **H$_2$L^1** complexes.

When the TGA curves of the complexes are examined, it is seen that [Co(**L**^{1})(H_2O)]·H_2O and [Ni(**L**^{1})(H_2O)]·2H_2O begin to decompose between 200 and 250 °C, [Cu(**L**^{1})(H_2O)] around 300 °C, and [Zn(**L**^{1})(H_2O)]·H_2O and K[Pd(**L**^{1})Cl] decompose above 350 °C. As for the complexes derived from **H$_2$L^2**; it is observed that [Ni(**L**^{2})(H_2O)] and [Co(**L**^{2})(H_2O)]·H_2O decompose around 300 °C; [Zn(**L**^{2})(H_2O)] and K[Pd(**L**^{2})Cl] above 200 °C. Decomposition temperature of [Cu(**L**^{2})(H_2O)] is above 350 °C. Decomposition point measurements are also compatible with these observations. From the differential thermal analysis (DTA) curves, the degradation degrees of the complexes can be determined. Figures 8 and S20 show the TGA and DTA curves of K[Pd(**L**^{1})Cl] and [Cu(**L**^{2})(H_2O)] complexes, respectively. The endothermic values observed at 381 °C for K[Pd(**L**^{1})Cl] and 361 °C for [Cu(**L**^{2})(H_2O)] as sharp peaks indicate the decomposition temperatures of these complexes. For other complex compounds, degradation degrees according to DTA are given in the experimental section.

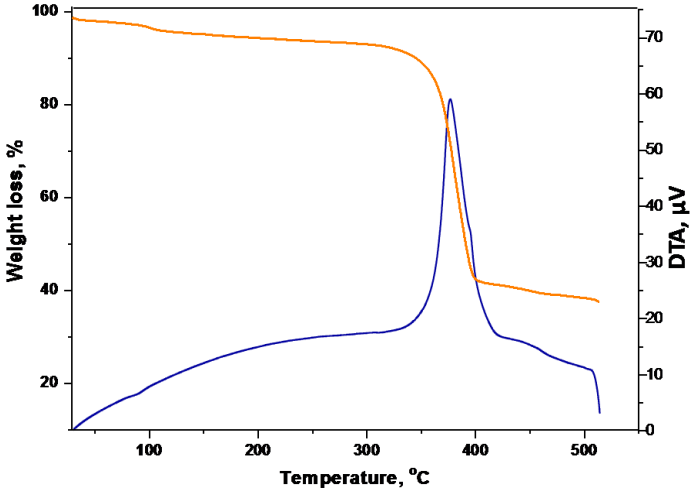

Fig. 8 – TGA and DTA curves of K[Pd(**L**^{1})Cl]

UV-visible spectroscopy

UV-visible spectral data of the compounds obtained in ethanol are presented in Experimental section. UV-visible spectral curves of **H**$_2$**L**^{1} and its complexes are given in Fig. 9, and those of **H**$_2$**L**^{2} and its complexes are given as supporting information (Fig. S21).

The electronic spectra of the compounds exhibit intense bands at the 200 – 290 nm region: The bands between 200 and 250 nm are due to $\pi \rightarrow \pi^*$ transitions in the aromatic rings. The bands at the 250 – 300 nm range correspond to $\pi \rightarrow \pi^*$ transitions of azomethine group, whereas the bands just above 300 nm correspond to the $n \rightarrow \pi^*$ transitions.[31]

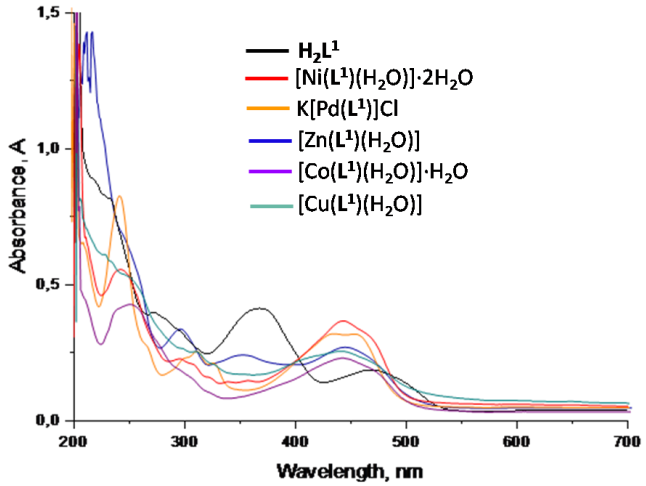

Fig. 9 – The UV-visible spectra of **H**$_2$**L**^{1} and its complexes in EtOH.

The 440 – 500 nm range bands seen in the ligands are related to intraligand charge transfer transitions. The bands at 350 – 550 nm range are due to d-d transitions and indicate square planar stereochemistry in solution for the complexes. For instance, the bands at 456 nm for K[Pd(**L**^{2})Cl] and at 469 nm for [Ni(**L**^{2})(H$_2$O)] can be assigned to $^1A_{1g} \rightarrow {}^1A_{2g}$ transition. The absorptions seen at 470 nm in both Co(II) complexes can be attributed to the $^1A_{1g} \rightarrow {}^1B_{1g}$ transition, which is one of the transitions specific to low spin square planar complexes. The bands at the 440 – 500 nm range for the Cu(II) complexes, which can be attributed to d-d transitions, may be considered as an indication that the complexes have distorted square pyramidal geometry.[32,33] Since there are no allowed d-d transitions in Zn(II) complexes, the bands at the 350 – 500 nm range arise from the intraligand and metal-to-ligand charge transfer transitions.

In the light of the analytical and spectroscopic data obtained, the structure in Figure 10 can be suggested for the synthesized complexes in the study.

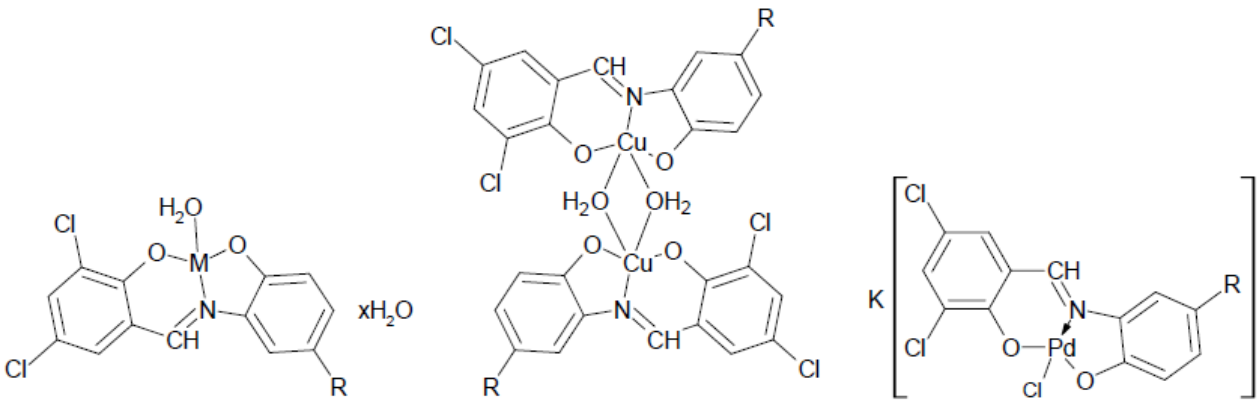

Fig. 10 – The proposed structures of the synthesized complexes in the study
(R: Cl, *tert*-Bu; M: Co(II), *x*:1; Ni(II), *x*: 0; Zn(II), *x*:0).

Antimicrobial activity

In vitro antimicrobial activity test results of $\mathbf{H_2L^1}$ and $\mathbf{H_2L^2}$ and their metal complexes in terms of MIC are presented in Table 2 in comparison with the values of the antibiotics and antifungal agents.

Table 2

In vitro antimicrobial activity of the compounds (MIC, µg/mL)

Compound	----------Bacteria----------						-------Fungi------		
	Sa[*,a]	*Se*[a]	*Kp*[b]	*Ec*[b]	*Pm*[b]	*Pa*[b]	*Cp*	*Ct*	*Ca*
$\mathbf{H_2L^1}$	625	312	312	625	625	–	625	156	312
$\mathbf{H_2L^2}$	625	625	–	625	312	625	312	625	1250
[Co($\mathbf{L^1}$)(H_2O)]·H_2O	312	625	625	156	312	625	1250	1250	625
[Ni($\mathbf{L^1}$)(H_2O)]·$2H_2O$	1250	625	312	1250	1250	625	1250	312	312
[Cu($\mathbf{L^1}$)(H_2O)]	625	625	312	312	625	312	1250	1250	625
[Zn($\mathbf{L^1}$)(H_2O)]	1250	625	625	156	312	625	312	625	156
K[Pd($\mathbf{L^1}$)Cl]	312	312	625	625	1250	625	625	625	156
[Co($\mathbf{L^2}$)(H_2O)]·H_2O	625	625	625	625	1250	-	625	625	625
[Ni($\mathbf{L^2}$)(H_2O)]	625	625	625	625	1250	1250	625	625	312
[Cu($\mathbf{L^2}$)(H_2O)]	312	156	625	625	1250	-	625	1250	625
[Zn($\mathbf{L^2}$)(H_2O)]	312	625	312	625	-	1250	625	625	625
K[Pd($\mathbf{L^2}$)Cl]	1250	625	312	625	625	625	625	625	312
References[c]	0.25	0.25	0.007	0.007	0.125	0.007	0.5	1.0	1.0

[*] *Sa* – *Staphylococcus aureus* ATCC 6538; *Se* – *Staphylococcus epidermidis* ATCC 12228; *Ec* – *Escherichia coli* ATCC 8739; *Kp* – *Klebsiella pneumoniae* ATCC 4352; *Pa* –*Pseudomonas aeruginosa* ATCC 1539; *Pm* – *Proteus mirabilis* ATCC 14153; *Ca* – *Candida albicans* ATCC 10231; *Cp* – *Candida parapsilosis* ATCC 22019; *Ct* – *Candida tropicalis* ATCC 750
[a]: Gram+; [b]: Gram–. - : No antimicrobial effect at 5000 µg/mL and lower dilutions
[c]: Ciprofloxacin and Amphotericin B were used for bacteria and fungi, respectively.

It is seen that the all the complexes show moderate or weak activity against the test microorganisms. It was observed that some of the complexes showed higher activity than the ligands,

as was the effect of copper(II) complex of $\mathbf{H_2L^2}$ against *Staphylococcus aureus* and *Staphylococcus epidermidis* (Gram+ bacteria). It is also notable that cobalt(II) and zinc(II) complexes of $\mathbf{H_2L^1}$ performed better against *Escherichia coli* than the ligand. It is also an important finding that $\mathbf{H_2L^1}$ does not show activity against *Pseudomonas aeruginosa* and $\mathbf{H_2L^2}$ against *Klebsiella pneumoniae*, however most of the complexes are effective.

Antiviral activity assay

Antiviral activity of the compounds was tested against Parainfluenza Type-2 virus and the results are given at Table 3. It was found that while $\mathbf{H_2L^1}$ inhibited viruses by 46%, $\mathbf{H_2L^2}$ was effective at a rate of 63%. Considering that $\mathbf{H_2L^1}$ contains chlorine atom and $\mathbf{H_2L^2}$ contains *tert*-butyl group at the same position, it is possible to say that the *tert*-butyl group gives Schiff base a higher virus inhibition feature.

It was observed that inhibition rate in the copper(II) and nickel(II) complexes of $\mathbf{H_2L^1}$ was increased compared to the ligand whereas those of the other complexes decreased. In all complexes of $\mathbf{H_2L^2}$, the antiviral effect was significantly reduced compared to the ligand.

Table 3

Antiviral activity of the compounds

Compound	Virus Inhibition, %
$\mathbf{H_2L^1}$	46
$\mathbf{H_2L^2}$	63
[Co($\mathbf{L^1}$)(H_2O)]·H_2O	37
[Ni($\mathbf{L^1}$)(H_2O)]·$2H_2O$	56
[Cu($\mathbf{L^1}$)(H_2O)]	56
[Zn($\mathbf{L^1}$)(H_2O)]	28
K[Pd($\mathbf{L^1}$)Cl]	39
[Co($\mathbf{L^2}$)(H_2O)]·H_2O	30
[Ni($\mathbf{L^2}$)(H_2O)]	26
[Cu($\mathbf{L^2}$)(H_2O)]	23
[Zn($\mathbf{L^2}$)(H_2O)]	33
K[Pd($\mathbf{L^2}$)Cl]	40
Ribavirin*	100

Ribavirin: Reference antiviral agent

EXPERIMENTAL

Chemistry and apparatus

All chemicals and solvents were of reagent grade and they were used without further purification.

The devices and techniques used are following: Elemental analysis: LECO combustion analyzer CHNS-932. Melting points: Buchi M-560 melting-point apparatus. Molar conductivity: WTW Cond315i conductivity meter (in DMF at 25 °C). Magnetic measurements: MK1 Sherwood Scientific apparatus (at room temperature by Gouy's method. Diamagnetic corrections were calculated using Pascal's constants). NMR spectroscopy: Varian Unity Inova 500 NMR spectrometer. FT-IR spectroscopy: Bruker Optics Vertex 70 spectrometer with Attenuated Total Reflection (ATR) techniques, between 400 and 4000 cm^{-1}. Mass spectrometry: Thermo Finnigan LCQ Advantage MAX LC/MS/MS (in positive ion mode). UV-Visible spectra were performed on Shimadzu UV-1800 Spectrophotometer in EtOH. Thermogravimetric studies were made on a TG-60WS Shimadzu, between 30 and 525 °C, with a heating rate of 10 °C/min and air flowing at the rate of 50 mL/min. ESI-MS in MeOH.

Synthesis of the ligands: general procedure

3,5-Dichlorosalicyladehyde (0.96 g, 5 mmol) and 2-amino-4-chlorophenol (0.72 g, 5 mmol) or 2-amino-4-*tert*-butylphenol (0.83 g, 5 mmol) were separately dissolved in absolute ethanol (10 mL), then they were mixed and refluxed for 3 h. The reaction mixture was cooled at room temperature; completion of the reaction was checked by TLC. After a few days, the crystals formed were filtered and dried at room temperature.

2,4-Dichloro-6-{(E)-[(5-chloro-2-hydroxyphenyl)imino]methyl}phenol **($\mathbf{H_2L^1}$):** $C_{13}H_8Cl_3NO_2$. MW: 316.57 g/mol. Dark orange solid. Yield: 85%. M.p.: 263 °C. ESI-MS (m/z, %): 278.9 ($[M\text{-}Cl\text{-}2H]^+$, 100), 316.9 ($[M]^+$, 12.1). FT-IR Spectra ($cm^{-1}$): 3050 – 2600 br (H-bonding), 3051 m $\nu(CH)_{arom.}$, 1626 m $\nu(HC=N)_{azomethine}$, 1602 m $\nu(C=C)_{arom}$, 1495 m, 1436 m, 1299 m, 1206 s $\nu(C–O)$, 1144 m, 1037 m, 847 m, 815 m $\delta(CH_{ar.})$, 750 m, 651 m, 571 m, 505 m, 451 m. ^{1}H-NMR (ppm, 500 MHz): 10.40 s (1H, OH), 9.09 s (1H, N=CH), 7.71 d (1H, J=2.6, H3), 7.64 d (1H, J=2.6, H5), 7.60 d (1H, J=2.6, H6'), 7.23 dd (1H, J=8.7, 2.5, H4'), 7.01 d (1H, J=8.7, H3'). ^{13}C-NMR (ppm, 125 MHz, DMSO-d_6): 161.1 (N=CH), 158.3 (C1–OH), 150.6 (C2'–OH), 133.7 (C1'), 132.9 (C3), 130.9 (C4'), 128.9 (C4), 123.7 (C5), 122.9 (C2), 121.4 (C5'), 120.4 (C6'), 119.4 (C3'), 118.5 (C6). UV-vis spectra (in EtOH, λ_{max}/nm): 203 m, 233 m,br, 272 m,br, 366 m,br, 470 m,br, 499 sh.

2-{(E)-[(5-tert-butyl-2-hydroxyphenyl)imino]methyl}-4,6-dichlorophenol **($\mathbf{H_2L^2}$):** $C_{17}H_{17}Cl_2NO_2$. MW: 338.23 g/mol. Orange solid. Yield: 85%. M.p.: 238 °C. ESI-MS (m/z, %): 338.3 ($[M]^+$, 60.9), 340.3 ($[M+2H]^+$, 37.2). FT-IR Spectra (cm^{-1}): 3188 m,br $\nu(OH)$, 3051 m $\nu(CH)_{arom.}$, 2957 m $\nu(CH)_{aliph}$, 2866 m $\nu(CH)_{aliph.}$,1635 m $\nu(HC=N)_{azomethine}$, 1611 m $\nu(C=C)_{arom.}$, 1503 s, 1359 m, 1284 m, 1217 m $\nu(C–O)$, 1139 m, 1005 m, 852 m, 820 m $\delta(CH)_{arom.}$, 755 m, 679 m, 579 m, 499 m, 435 m. ^{1}H-NMR (ppm, 500 MHz): 10.01 s (1H, OH),

9.15 s (1H, N=CH), 7.65 d (1H, J=2.6, H3), 7.64 d (1H, J=2.4, H5), 7.51 d (1H, J=2.4, H6'), 7.22 dd (1H, J=8.3, 2.6, H4'), 6.94 d (1H, J=8.3, H3'), 1.30 s (9H, -C(CH_3)$_3$). ^{13}C-NMR (ppm, 125 MHz, DMSO-d_6): 160.5 (N=CH), 159.0 (C1–OH)), 148.9 (C2'–OH), 142.8 (C1'), 132.8 (C3), 130.8 (C4'), 130.5 (C5), 126.5 (C4), 123.6 (C2), 120.0 (C5'), 119.9 (C6'), 116.6 (C3'), 116.2 (C6), 34.5 (–C(CH_3)$_3$), 31.7 (–C(CH_3)$_3$). UV-vis spectra (in EtOH, λ_{max}/nm): 205 s, 215 m, 242 m,br, 305 m,br, 365 m,br, 468 m,br.

Synthesis of the complex compounds

Appropriate metal salt solutions (1 mmol of Co(II), Ni(II), Cu(II), Zn(II) perchlorates and K_2PdCl_4, e.g. 366 mg of $Co(ClO_4)_2{\cdot}6H_2O$) was added gradually to a solution of the ligand (1 mmol, e.g. 317 mg of **H_2L^1**) in 15 mL of EtOH and heated to reflux for 3 hours. K_2PdCl_4 solution was obtained by dissolving 1 mmol $PdCl_2$ and 2 mmol KCl in 10 mL EtOH+water mixture (7:3, v/v). While Cu(II) and Pd(II) salts immediately precipitated with the ligands, Co(II), Ni(II) and Zn(II) salts formed solutions, no precipitate was formed under the reaction conditions. The solution of NaOH in 5% ethanol was added to the solutions of Co(II), Ni(II) and Zn(II) complexes dropwise and the pH of the solution was brought to around 5. Then, the precipitates were obtained from the solution kept at room temperature. The precipitates were filtered, dried and crystallized again from ethanol. It was dried at room temperature.

[Co(L^1)(H$_2$O)]·H$_2$O: Dark red solid, yield: 70%. Decomposition point (Dec.p.).: >225 °C. Calcd. for $C_{13}H_{10}Cl_3NO_4Co$ (%): C, 38.13; H, 2.46; N, 3.42. Found (%): C, 38.80; H, 2.84; N, 3.40. MW: 409.51 g/mol. μ_{eff} = 1.42 BM. Molar conductivity: 19.3 $\Omega^{-1}cm^2mol^{-1}$. FT-IR spectroscopy (cm^{-1}): 3509 m,br ν(H_2O), 3242 m,br ν(OH), 3073 w ν(CH)$_{arom.}$, 1620 m ν(HC=N)$_{azomethine}$, 1575 m ν(C=C)$_{arom.}$, 1494 m, 1410 m, 1366 m, 1252 m, 1212 m ν(C–O), 1139 m, 1078 m, 912 m, 859 m, 815 m δ(CH)$_{arom.}$, 744 m, 669 m, 606 m, 575 m, 527 m, 499 m, 413 m. UV-vis spectra (in EtOH, λ_{max}/nm): 204 m, 209 sh, 251 m,br, 300 w, 440 m,br, 470 sh. TGA (temp., °C: weight loss, %): 50: 4.3; 75: 5.1 (1 mole of H_2O); 100: 5.5; 150: 7.7; 200: 10.4 (2 moles of H_2O); 250: 21.6; 300: 37.1; 350: 51.9; 400: 55.6; 450: 58.6; 500: 65.7. DTA (°C): 212, 232, 475.

[Ni(L^1)(H$_2$O)]·2H$_2$O: Dark yellow solid, yield: 67%. Dec.p.: >250 °C. Calcd. for $C_{13}H_{12}Cl_3NO_5Ni$ (%): C, 36.54; H, 2.83; 3.28. Found (%): C, 35.50; H, 2.51; N, 3.03. MW: 427.3 g/mol. μ_{eff} = 2.33 BM. Molar conductivity: 33.0 $\Omega^{-1}cm^2mol^{-1}$. FT-IR spectroscopy (cm^{-1}): 3511 ν(H_2O), 3218 m,br ν(OH), 3070 m,br ν(CH)$_{arom.}$, 1621 m ν(HC=N)$_{azomethine}$, 1587 m ν(C=C)$_{arom.}$, 1493 m, 1354 m, 1210 m ν(C–O), 1117 m, 1082 m, 920 m, 861 m, 813 m δ(CH)$_{arom.}$, 759 s, 624 m, 606 m, 530 m, 503 m, 426 m. UV-vis spectra (in EtOH, λ_{max}/nm): 205 s, 209 m, 239 m, 295 m,br, 308 w, 442 m,br, 468 sh. TGA (temp., °C: weight loss, %): 50: 7.3; 75: 8.5 (2 moles of H_2O); 100: 9.0; 150: 13.1 (3 mole of H_2O); 200: 14.7; 250: 20.5; 300: 34.2; 350: 38.2; 400: 41.4; 450: 54.6; 500: 63.6. DTA (°C): 259, 443, 514.

[Cu(L$_1$)(H$_2$O)]: Khaki green solid. Yield: 74%. Dec.p.: >300 °C. Calcd. for $C_{13}H_8Cl_3NO_3Cu$ (%): C, 39.42; H, 2.04; N, 3.54. Found (%): C, 41.00; H, 1.88; N, 3.50. MW: 396.1 g/mol. μ_{eff} = 1.22 BM. Molar conductivity: 1.2 $\Omega^{-1}cm^2mol^{-1}$. FT-IR spectroscopy (cm^{-1}): 3193 m,br ν(OH), 3087 m,br ν(CH)$_{arom.}$, 1626 m ν(HC=N)$_{azomethine}$, 1596 w ν(C=C)$_{arom.}$, 1505 m, 1457 s, 1373 m, 1297 m, 1241 m ν(C–O), 1092 m, 1064 s, 935 m, 859 m, 806 s δ(CH)$_{arom.}$, 763 m, 733 m, 667 m, 596 m, 512 m, 489 m, 426 m. UV-vis spectra (in EtOH, λ_{max}/nm): 202 s, 206 m, 251 sh, 310 w, 410 sh, 441 m,br. TGA (temp., °C: weight loss, %): 50: 0.6; 75: 1.4; 100: 2.0; 150: 3.6; 200: 4.6 (1 mole H_2O); 250: 8.3; 300: 17.1; 350: 23.6; 400: 32.0; 450: 64.4; 500: 81.6. DTA (°C): 269, 417.

[Zn(L^1)(H$_2$O)]: Dark yellow solid. Yield: 73%. Dec.p.: >350 °C. Calcd. for $C_{13}H_8Cl_4NO_3Zn$ (%): C, 39.23; H, 2.03; N, 3.52. Found (%): C, 40.40; H, 1.95; N, 3.38. MW: 398.0 g/mol. Molar conductivity: 3.0 $\Omega^{-1}cm^2mol^{-1}$. FT-IR spectroscopy (cm^{-1}): 3206 m,br ν(OH), 3087 m ν(CH)$_{arom.}$, 1633 m ν(HC=N)$_{azomethine}$, 1603 m ν(C=C)$_{arom.}$, 1555 m, 1497 m, 1456 s, 1406 m, 1298 m, 1240 m ν(C–O), 1141 m, 1092 m, 1018 s, 938 m, 872 m, 807 m δ(CH)$_{arom.}$, 772 m, 736 m, 625 m, 597 m, 515 m, 429 m. ^{1}H-NMR spectroscopy (500 MHz): 8.97 s (1H, N=CH), 7.66 d (1H, J=2.4, H3), 7.49 d (2H, J=2.9, 2.9, H5+H6'), 7.03 dd (1H, J=8.7, 2.6, H4'), 6.99 s,br (H3'). ^{13}C-NMR (ppm, 125 MHz, DMSO-d_6): 164.1 (N=CH), 163.8 (C1–O), 153.7 (C2'–O), 138.9 (C1'), 133.2 (C3), 132.0 (C4'), 126.7 (C4), 125.7 (C5), 121.5 (C2), 121.1 (C5'), 117.7 (C6'), 115.4 (C3'), 110.0 (C6). UV-vis spectra (in EtOH, λ_{max}/nm): 206 s, 209 m, 259 sh, 296 m,br, 382 m,br, 445 m,br, 470 sh. TGA (temp., °C: weight loss, %): 50: 0.7; 75: 1.1; 100: 1.8; 150: 2.7; 200: 4.3 (1 mole of H_2O); 250: 4.8; 300: 5.3; 350: 6.0; 400: 7.1; 450: 14.5; 500: 46.3. DTA (°C): 452, 471.

K[Pd(L^1)Cl]: Light brown solid. Yield: 74%. Dec.p.:>350 °C. Calcd. for $C_{13}H_6Cl_4KNO_2Pd$ (%): C, 31.51; H, 1.22; N, 2.83. Found (%): C, 30.90; H, 1.56; N, 2.84. MW: 495.52 g/mol. Molar conductivity: 29.2 $\Omega^{-1}cm^2mol^{-1}$. FT-IR spectroscopy (cm^{-1}): 3064 m ν(CH)$_{arom.}$, 1637 m ν(HC=N)$_{azomethine}$, 1591 m ν(C=C)$_{arom.}$, 1479 s, 1433 m, 1370 m, 1270 m, 1214 m ν(C–O), 1176 s, 1088 m, 926 m, 835 m δ(CH)$_{arom.}$, 768 m, 709 m, 664 m, 549 s, 519 m, 465 m, 423 m. ^{1}H-NMR spectroscopy (500 MHz, ppm): 8.76 s (1H, N=CH), 7.96 d (1H, J=2.2, H3), 7.70 d (1H, J=2.6, H5), 7.55 d (1H, J=2.6, H6'), 7.02 dd (1H, J=8.8, 2.3, H4'), 6.69 d (1H, J=8.8, H3'). ^{13}C-NMR (ppm, 125 MHz, DMSO-d_6): 167.2 (N=CH), 156.8 (C1–OH), 147.3 (C2'–OH), 140.2 (C1'), 132.3 (C3), 128.8 (C4'), 126.1 (C4), 123.1 (C5), 119.2 (C2), 119.0 (C5'), 118.1 (C6'), 116.7 (C3'), 116.4 (C6). UV-vis spectra (in EtOH, λ_{max}/nm): 206 s, 211 m, 244 m, 268 sh, 300 sh,313 m,br, 328 m,br, 435 m,br, 454 m,br. TGA (temp., °C: weight loss, %): 50: 0.7; 75: 1.0; 100: 1.3; 150: 2.5; 200: 4.7; 250: 6.3; 300: 7.2; 350: 10.9; 400: 57.6; 450: 60.1; 500: 61.6. DTA (°C): 381.

[Co(L^2)(H$_2$O)]·H$_2$O: Brownish red solid. Yield: 68%. Dec.p.: >300 °C. Calcd. for $C_{17}H_{19}Cl_2NO_4Co$ (%): C, 47.35; H, 4.44; N, 3.25. Found (%): C, 46.82; H, 4.28; N, 3.07. MW: 431.18 g/mol. μ_{eff} = 1.54 BM. Molar conductivity: 21.3 $\Omega^{-1}cm^2mol^{-1}$. FT-IR spectroscopy (cm^{-1}): 3487 m,br ν(H_2O), 3231 m,br ν(OH), 3068 w ν(CH)$_{arom.}$, 2957 m ν(CH)$_{aliph}$, 2867 m ν(CH)$_{aliph.}$, 1639 m ν(HC=N)$_{azomethine}$, 1615 m ν(C=C)$_{arom.}$, 1491 m, 1434 m, 1363 m, 1250 m, 1224 m ν(C–O), 1121 m, 1091 m, 1078 s, 822 m δ(CH)$_{arom.}$, 784 m, 736 m, 625 m, 545 m, 499 m, 443 m, 425 m. UV-vis spectra (in EtOH, λ_{max}/nm): 203 s, 206 m, 249 m,br, 277 sh, 438 m,br, 470 sh. TGA (temp., °C: weight loss, %): 50: 1.9; 75: 2.7; 100: 3.6 (1 mole H_2O); 150: 5.7; 200: 8.2 (2 moles of H_2O; 250: 9.0; 300: 12.2; 350: 21.1; 400: 25.6; 450: 47.5; 500: 58.7. DTA (°C): 222, 316, 427.

[Ni(L²)(H₂O)]: Dark yellow solid. Yield: 71%. Dec.p.: >300 °C. Calcd. for $C_{17}H_{17}Cl_2NO_3Ni$ (%): C, 49.45; H, 4.15; N, 3.39. Found (%): C, 49.30; H, 4.21; N, 3.21. MW: 412.9 g/mol. μ_{eff} = 2.26 BM. Molar conductivity: 21.1 $\Omega^{-1}cm^2mol^{-1}$. FT-IR spectroscopy (cm^{-1}): 3285 m,br ν(OH), 3071 m $\nu(CH)_{arom.}$, 2965 m $\nu(CH)_{aliph.}$, 2869 m $\nu(CH)_{aliph.}$, 1625 m $\nu(HC=N)_{azomethine}$, 1580 m $\nu(C=C)_{arom.}$, 1508 m, 1418 m, 1367 m, 1268 m, 1216 m ν(C–O), 1201 m, 1164 m, 1125 m, 938 m, 864 m, 824 m $\delta(CH)_{arom.}$, 757 s, 624 m, 608 m, 542 m, 499 s, 470 m, 419 m. UV-vis spectra (in EtOH, λ_{max}/nm): 204 s, 210 m, 237 m,br, 298 m,br, 312 m,br, 326 m, 374 sh, 441 m,br, 469 m,br. TGA (temp., °C: weight loss, %): 50: 1.1; 75: 1.4; 100: 1.6; 150: 4.6 (1 mole of H_2O); 200: 7.4; 250: 10.1; 300: 20.1; 350: 40.0; 400: 58.8; 450: 73.0; 500: 81.2. DTA (°C): 397, 454.

[Cu(L²)(H₂O)]: Khaki green solid. Yield: 76%. Dec.p.: >350 °C. Calcd. for $C_{17}H_{17}Cl_2NO_3Cu$ (%): C, 48.87; H, 4.10; N, 3.35. Found (%): C, 49.20; H, 3.86; N, 3.27. MW: 417.8 g/mol. μ_{eff} = 1.11 BM. Molar conductivity: 2.1 $\Omega^{-1}cm^2mol^{-1}$. FT-IR spectroscopy (cm^{-1}): 3225 m,br ν(OH), 3067 m $\nu(CH)_{arom.}$, 2955 m $\nu(CH)_{aliph.}$, 2869 m $\nu(CH)_{aliph.}$, 1645 m $\nu(HC=N)_{azomethine}$, 1610 m $\nu(C=C)_{arom.}$, 1567 m, 1490 s, 1442 m, 1361 m, 1254 s, 1222 m ν(C–O), 1096 m, 954 m, 821 m $\delta(CH)_{arom.}$, 735 m, 622 m, 542 m, 497 m, 454 m, 429 m. UV-vis spectra (in EtOH, λ_{max}/nm): 203 s, 210 m, 237 m, 269 m,br, 313 w, 449 m,br, 482 m,br. TGA (temp., °C: weight loss, %): 50: 0.4; 75: 0.8; 100: 1.4; 150: 4.4 (1 mole of H_2O); 200: 4.6; 250: 5.6; 300: 6.1; 350: 7.2; 400: 30.1; 450: 44.3; 500: 57.5. DTA (°C): 362, 431, 506.

[Zn(L²)(H₂O)]: Light brown solid. Yield: 67%. Dec.p.: >250 °C. Calcd. for $C_{17}H_{17}Cl_2NO_3Zn$ (%): C, 48.66; H, 4.08; N, 3.34. Found (%): C, 47.90; H, 3.14; N, 3.24. MW: 419.64 g/mol. Molar conductivity: 21.0 $\Omega^{-1}cm^2mol^{-1}$. FT-IR spectroscopy (cm^{-1}): 3223 m,br ν(OH), 3065 w,br $\nu(CH)_{arom.}$, 2966 m $\nu(CH)_{aliph.}$, 2869 m $\nu(CH)_{aliph.}$, 1654 m $\nu(HC=N)_{azomethine}$, 1616 m $\nu(C=C)_{arom.}$, 1563 m, 1482 m, 1455 m, 1364 m, 1243 m ν(C–O), 1195 m, 1081 m, 1046 s, 871 m, 789 m $\delta(CH)_{arom.}$, 735 s, 652 m, 620 m, 513 m, 458 m, 424 m. ^{1}H-NMR spectroscopy (500 MHz, ppm): 8.94 (1H, N=CH), 7.56 s (1H, H3), 7.52 s (1H, H5), 7.41 s (1H, H6'), 7.07 s,br (1H, H4'), 6.87 s,br (1H, H3'), 1.27 s (9H, -$C(CH_3)_3$). ^{13}C-NMR (ppm, 125 MHz, DMSO-d_6): 165.0 (N=CH), 163.7 (C1–O)), 138.8 (C2'–O), 136.9 (C1'), 134.8 (C3), 133.6 (C4'), 131.4 (C5), 127.1 (C4), 122.4 (C2), 120.81 (C5'), 115.3 (C6'), 114.6 (C3'), 113.3 (C6), 32.6 (–$C(CH_3)_3$), 31.8 (–$C(CH_3)_3$). UV-vis spectra (in EtOH, λ_{max}/nm): 204 s, 206 s, 215 sh, 233 m,br, 300 m,br, 331 w, 367 m,br, 442 m,br, 467 sh. TGA (temp., °C: weight loss, %): 50: 0.2; 75: 1.5; 100: 1.8; 150: 3.7 (1 mole of H_2O); 200: 11.3; 250: 27.9; 300: 39.6; 350: 44.7; 400: 54.4; 450: 61.2; 500: 79.2. DTA (°C): 245, 351, 482.

K[Pd(L²)Cl]: Light brown solid. Yield: 72%. Dec.p.: >200 °C. Calcd. for $C_{17}H_{15}Cl_3KNO_2Pd$ (%): C, 39.48; H, 2.92; N, 2.71. Found (%): C, 39.11; H, 3.07; N, 2.67. MW: 517.18 g/mol. Molar conductivity: 28.0 $\Omega^{-1}cm^2mol^{-1}$. FT-IR spectroscopy (cm^{-1}): 3061 m $\nu(CH)_{arom.}$, 2971 m $\nu(CH)_{aliph.}$, 2871 m $\nu(CH)_{aliph.}$, 1637 m $\nu(HC=N)_{azomethine}$, 1594 m $\nu(C=C)_{arom.}$, 1480 s, 1437 m, 1372 m, 1306 m, 1217 m ν(C–O), 1175 s, 1088 m, 926 m, 834 m $\delta(CH)_{arom.}$, 771 m, 742 m, 664 m, 549 s, 462 m, 446 m, 422 m. ^{1}H-NMR spectroscopy (ppm, 500 MHz): 8.77 s (1H, N=CH), 7.84 s (2H, H3+H5), 7.53 s (1H, H6'), 7.07 d (1H, J=9.4, H4'), 6.62 d (1H, J=8.9, H3'), 1.30 s (9H, –$C(CH_3)_3$). ^{13}C-NMR (ppm, 125 MHz): 166.5 (N=CH), 156.3 (C1–OH), 139.0 (C2'–OH), 137.3 (C1'), 132.7 (C3), 131.4 (C4'), 125.9 (C4), 123.5 (C5), 117.9 (C2), 117.2 (C5'), 116.5 (C6'), 113.8 (C3'), 112.4 (C6), 32.6 (–$C(CH_3)_3$), 31.8 (–$C(CH_3)_3$). UV-vis spectra (in EtOH, λ_{max}/nm): 205 s, 214 m, 244 m, 268 sh, 300 sh, 315 m,br, 329 sh, 436 m,br, 456 m,br. TGA (temp., °C: weight loss, %): 50: 0.1; 75: 0.5; 100: 1.1; 150: 3.5; 200: 21.1; 250: 34.6; 300: 44.1; 350: 54.2; 400: 56.7; 450: 56.7; 500: 56.8. DTA (°C): 212, 278.

Determination of antibacterial and antifungal activity

Antimicrobial activities of the complex compounds were investigated against bacteria and fungi by the microbroth dilutions way according to the Clinical and Laboratory Standards Institute (CLSI) guidance.[35-37] The antimicrobial activity procedure and the microorganisms used are the same as in our previous studies.[8,38]

Antiviral activity assay

For Parainfluenza Type-2 virus (PIV-2), African green monkey kidney cell line (VERO, ATCC) was cultured in Dulbecco's modified Eagle's medium (Wisent, MULTICELL) supplemented with 10% fetal bovine serum (FBS; Sigma), 100 U/mL penicillin, and 100 μg/mL streptomycin. The PIV-2 and cells were maintained at 37°C under 5% CO_2 atmosphere.

An experiment was conducted based on the plaque formation test for PIV-2 strain that grown on VERO cell culture.[39] VERO cells were infected with PIV-2 at 100 PFU per well, one of the wells was used as a control and the antiviral activities of the samples were tested in the other wells. The virus-infected control (Ribavirin) well was accepted as 100%, and the efficacy results were calculated as a percentage by comparing this control value. The concentration of the compounds is 10 mg/mL.

X-ray single crystal diffraction analysis

H_2L^1 and **H_2L^2** were crystallized from EtOH. The orange colored single crystals were obtained for both ligand. Suitable crystals of **H_2L^1** and **H_2L^2** were selected for data collection which was performed on a Bruker-D8 QUEST diffractometer equipped with a graphite-monochromatic Mo-K_α radiation at 296 K. The structures were solved by direct methods using SHELXS-2013[40] and refined by full-matrix least-squares methods on F^2 using SHELXL-2013.[41] All non-hydrogen atoms were refined with anisotropic parameters. The H atoms of C atoms were located from different maps and then treated as riding atoms with C–H distance of 0.93 – 0.97 Å. The other H atoms were located in a difference map refined freely. The following procedures were implemented in our analysis: data collection: Bruker APEX2;[42] program used for molecular graphics were as follow: MERCURY programs;[43] software used to prepare material for publication: WinGX.[44] Details of data collection and crystal structure determinations are given in Table 1. Crystallographic data for the structural analysis are deposited with the Cambridge Crystallographic Data Centre, CCDC No. 2194774 and 2194769, for **H_2L^1** and **H_2L^2**, respectively.

CONCLUSION

Schiff bases derived from salicylaldehyde are compounds that attract attention due to their chelation structures as ligands, their variety of uses, and many interesting properties. In this context, we synthesized two new salicyl based Schiff bases derived from 3,5-dichlorosalicylaldehyde and 4-(chloro/*tert*-butyl)-2-aminophenols (**H_2L^1** and **H_2L^2**) and characterized by single-crystal X-ray diffraction and the other physicochemical and spectral techniques. Then, we prepared the complexes of **H_2L^1** and **H_2L^2** with Co(II), Ni(II), Cu(II), Zn(II) perchlorates and K_2PdCl_4, and characterized with elemental analysis, molar conductivity, magnetic moment, TGA, UV-visible, FT-IR and NMR spectroscopy. Based on the data, it was suggested that the complex compositions were in the form of $[M(\mathbf{L}^n)(H_2O)]\cdot xH_2O$ {M(II) = Co(II) (n = 1, 2; x = 1), Ni(II) (n = 1, x = 2; n = 2, x = 0), Cu(II) (n = 1, 2; x = 0), Zn(II) (n = 1, 2; x = 0)} and $K[Pd(\mathbf{L}^n)Cl]$ (n = 1, 2). All the complexes were found non-electrolyte characteristic with a 1:1 M:L ratio. The ligands and the complexes were tested against six bacteria, three fungi and Parainfluenza Type-2 virus. Overall, the compounds showed moderate antibacterial and antifungal activity. It was observed that some of the complexes exhibited higher activity against some microorganisms than the ligands. The higher antiviral effect of **H_2L^2** than **H_2L^1** can be evaluated as the *tert*-butyl group conferring a higher antiviral property to **H_2L^2**.

Acknowledgments: This work was supported by Scientific Research Projects Coordination Unit of Istanbul University-Cerrahpasa, Project number 36370.

REFERENCES

1. R. Sahu, D. S. Thakur and P. Kashyap, *Int. J. Pharm. Sci Nanotech.*, **2012**, *5*, 1757–1764.
2. a) S. K. Sridhar, M. Saravanan and A. Ramesh, *Eur. J. Med. Chem.*, **2001**, *36*, 615–625; b) P. Panneerselvam, R. R. Nair, G. Vijayalakshmi, E. H. Subramanian and S. K. Sridhar, *Eur. J. Med. Chem.*, **2005**, *40*, 225–229; c) J. Ceramella, D. Iacopetta, A. Catalano, F. Cirillo, R. Lappano and M. S. Sinicropi, *Antibiotics*, **2022**, *11*, Article ID 191; d) S. N. Pandeya, D. Sriram, G. Nath and E. DeClercq, *Eur. J. Pharmacol.*, **1999**, *9*, 25–31.
3. C. M. da Silva, D. L. da Silva, L. V. Modolo, R. B. Alves, M. A. de Resende, C. V. B. Martins and A. de Fatima, *J. Adv. Res.*, **2011**, *2*, 1–8.
4. A. Kajal, S. Bala, S. Kamboj, N. Sharma and V. Saini, *J. Catal.* **2013**, *2013*, Article ID 893512.
5. a) S. Ren, R. Wang, K. Komatsu, P. Bonaz-Krause, Y. Zyrianov, C. E. McKenna, C. Csipke, Z. A. Tokes and E. J. Lien, *J. Med. Chem.*, **2002**, *45*, 410–419; b) L. Shi, H.-M. Ge, S.-H. Tan, H.-Q. Li, Y.-C. Song, H.-L. Zhu and R.-X. Tan, *Eur. J. Med. Chem.*, **2007**, *42*, 558–564.
6. a) Ö. Celik, M. Ulusoy, E. Tas and S. Ide, *Anal. Sciences*, **2007**, *23*, x185–x186; b) H. E. Hashem, A. Nath and A. Kumar, *J. Mol. Struct.*, **2022**, *1250*, Article ID 131915; c) R. Kumar, A. A. Singh, U. Kumar, P. Jain, A. K. Sharma, C. Kant and M. S. H. Faizi, *J. Mol. Struct.*, **2023**, *1294*, Article ID 136346; d) P. G. Cozzi, *Chem. Soc. Rev.*, **2004**, *33*, 410–421; e) M. T. H. Tarafder, K. T. Jin, K. A. Crouse, A. M. Ali, B. M. Yamin and H.-K. Fun, *Polyhedron*, **2002**, *21*, 2547–2554.
7. E. Alterhoni, A. Tavman, D. Gürbüz, M. Hacioglu, A. Çinarli, O. Şahin and A. S. Birteksöz Tan, *ChemistrySelect*, **2020**, *5*, 9730–9735.
8. E. Alterhoni, A. Tavman, M. Hacioglu, O. Şahin and A. S. Birteksöz Tan, *J. Mol. Struct.*, **2021**, *1229*, Article ID 129498.
9. a) E. Fujita, B. S. Brunschwig, T. Ogata and S. Yanagida, *Coord. Chem. Rev.*, **1994**, *132*, 195–200; b) E. Kimura, S. Wada, M. Shiyonoya and Y. Okazaki, *Inorg. Chem.*, **1994**, *33*, 770–778; c) B. De Clercq and F. Verpoort, *Macromolecules*, **2002**, *35*, 8943–8947; d) T. Opstal and F. Verpoort, *Angew. Chem. Int. Ed.*, **2003**, *42*, 2876–2879; e) B. De Clercq, F. Lefebvre and F. Verpoort, *Appl. Catal.*, **2003**, *A247*, 345–364.
10. G. Tantaru, V. Dorneanu and M. Stan, *J. Pharm. Biomed. Anal.*, **2002**, *27*, 827–840.
11. a) M. Kumar, H. Agarkar and M. S. Degani, *J. Anal. Chem.*, **2023**, *78*, 866–877; b) D. M. Boghaei and S. Mohebi, *Tetrahedron* **2002**, *58*, 5357–5366.
12. a) S. Papic, N. Koprivanac, Z. Grabaric and D. Parac-Osterman, *Dyes Pigm.*, **1994**, *25*, 229–240; b) K. Nejati, Z. Rezvani and B. Massoumi, *Dyes Pigm.*, **2007**, *75*, 653–657.
13. S. Kumar, D. N. Dhar and P. N. Saxena, *J. Sci. Ind. Res.*, **2009**, *68*, 181–187.
14. a) M. M. H. Khalil, M. M. Aboaly and R. M. Ramadan, *Spectrochim. Acta*, **2005**, *A61*, 157–161; b) N. Chantarasiri, V. Ruangpornvisuti, N. Muangsin, H. Detsen, T. Mananunsap, C. Batiya and N. Chaichit, *J. Mol. Struct.*, **2004**, *701*, 93–103; c) S. M. Abdallah, G. G. Mohamed, M. A. Zayed and M. S. A. El-Ela, *Spectrochim. Acta*, **2009**, *A73*, 833–840.
15. a) D. Nartop, Ö. Özdemir and P. Gürkan, *Mor. J. Chem.*, **2017**, *5*, 560–572; b) N. Rasouli and P. Hyidari, *Mor. J. Chem.*, **2018**, *6*, 43–50.
16. a) A. Çinarli, D. Gürbüz, A. Tavman and A. S. Birteksöz, *Bull. Chem. Soc. Ethiop.*, **2011**, *25(3)*, 407–417. b) A. Çinarli, D. Gürbüz, A. Tavman and A. S. Birteksöz, *Chinese J. Chem.*, **2012**, *30(2)*, 449–459; c) D. Gürbüz, A. Çinarli, A. Tavman and A. S. Birteksöz, *Chinese J. Chem.*, **2012**, *30(4)*, 970–978.
17. a) D. Gürbüz, A. Çinarli, A. Tavman and A. S. Birteksöz Tan, *Bull. Chem. Soc. Ethiop.*, **2015**, *29(1)*, 63–74; b) K. I. Alexopoulou, E. Zagoraiou, T. F. Zafiropoulos, C. P. Raptopoulou, V. Psycharis, A. Terzis and S. P. Perlepes, *Spectrochim. Acta A*, **2015**, *136*, 122–130; c) B. S. Kusmariya and A. P. Mishra, *J. Mol. Struct.*, **2017**, *1130*, 727–738; d) Z.-J. Zhang, H.-T. Zeng, Y. Liu, D.-Z. Kuang, F.-X. Zhang, Y.-X. Tan and W.-J. Jiang, *Inorg. Nano-Metal Chem.*, **2018**, *48(10)*, 486–494.
18. Y.-X. Tan, Z.-J. Zhang, Y. Liu, J.-X. Yu, X.-M. Zhu, D.-Z. Kuang and W.-J. Jiang, *J. Mol. Struct.*, **2017**, *1149*, 874–881.

19. A. A. Abdel Aziz, A. N. M. Salem, M. A. Sayed and M. M. Aboaly, *J. Mol. Struct.*, **2012**, *1010*, 130–138.
20. M. M. Abo-Aly, A. M. Salem, M. A. Sayed and A. A. Abdel Aziz, *Spectrochim. Acta A*, **2015**, *136*, 993–1000.
21. N. P. Yahaya and M. S. Mukhtar, *Sci. J. Chem.*, **2021**, *9*, 9–13.
22. X. Totta, A. A. Papadopoulou, A. G. Hatzidimitriou, A. Papadopoulos and G. Psomas, *J. Inorg. Biochem.*, **2015**, *145*, 79–93.
23. A. Kerflani, K. S. Larbi, A. Rabahi, A. Bouchoucha, S. Zaater and S. Terrachet-Bouaziz, *Inorg. Chim. Acta*, **2022**, *529*, Article ID120659.
24. W. Geary, *J. Coord. Chem. Rev.*, **1971**, *7*, 81–122.
25. S. Amer, N. El-Wakiel and H. El-Ghamry, *J. Mol. Struct.*, **2013**, *1049*, 326–335.
26. I. A. Mantoo, M. Bashir and I. Yousuf, *Inorg. Chem. Commun.*, **2023**, *157*, Article ID 111384.
27. S. A. Carabineiro, Le. C. Silva, P. T. Gomes, L. C. J. Pereira, L. F. Veiros, S. I. Pascu, M. T. Duarte, S. Namorado and R. T. Henriques, *Inorg. Chem.*, **2007**, *46* (17), 6880–6890.
28. D. Lomjansky, C. Rajnak, J. Titis, J. Monco, L. Smolko and R. Boca, *Inorg. Chim. Acta*, **2018**, *483*, 352–358; A. G. Starikov, R. M. Minyaev and V. I. Minkin, *Chem. Phys. Lett.*, **2008**, *459*, 27–32; A. J. Bridgeman, *Dalton Trans.*, **2008**, *2008*, 1989–1992.
29. Q. Guan, P. Shi, J. B. Shen, H. D. Xian and G. L. Zhao, *J. Chem. Res.*, **2013**, *37(3)*, 131–135.
30. R. Knochenmuss and S. Leutwyler, *J. Chem. Phys.*, **1992**, *96(7)*, 5233–5244; B. Zhang, Y. Yu, Y. Y. Zhang, S. Jiang, Q. Li, H. S. Hu, G. Li, Z. Zhao, C. Wang, H. Xie, W. Zhang, D. Dai, G. Wu, D. H. Zang, L. Jiang, J. Li and X. Yang, *PNAS*, **2020**, *117*(27), 15423–15428.
31. Y. Kaya, H. Mutlu and G. Irez, *Gazi Univ. J. Sci.*, **2010**, *23(1)*, 13–18.
32. F. A. Mautner, R. C. Fischer, A. Torvisco, M. M. Henary, F. R. Louka, S. S. Massoud and N. M. Salem, *Molecules*, **2020**, *25*(15), Article ID 3376.
33. S. Khan, A. Al Masum, M. M. Islam, M. G. Drew, A. Bauzá, A. Frontera and S. Chattopadhyay, *Polyhedron*, **2017**, *123*, 334–343.
34. Clinical and Laboratory Standards Institute (CLSI), Methods for dilution antimicrobial susceptibility tests for bacteria that grow aerobically: Approved Standard M7-A5. Wayne, PA, USA, **2006**.
35. Clinical and Laboratory Standards Institute (CLSI), Reference method for broth dilution antifungal susceptibility testing of yeasts: Approved Standard M27-A2, 2nd Ed., Clinical Laboratory Standards, Wayne, PA, USA, **2002**.
36. Clinical and Laboratory Standards Institute, Performance standards for antimicrobial susceptibility testing; 24th informational supplement, M 100-S24:CLSI, Wayne, PA, USA, **2014**.
37. E. Alterhoni, A. Tavman, M. Hacioğlu, U. Şahintürk and A. S. Birteksöz Tan, *Jordan J. Chem.*, **2022**, *17*, 35–45.
38. K. Fukushima, T. Takahashi, M. Takaguchi, H. Ueyama, S. Ito, Y. Kurebayashi, T. Kawanishi, J. L. McKimm-Breschkin, T. Takimoto, A. Minami and T. Suzuki. *Biol. Pharm. Bull.*, **2011**, *34*, 996–1000.
39. G. M. Sheldrick, *Acta Cryst*., **2008**, *A64*, 112–122.
40. G. M. Sheldrick, *Acta Cryst*., **2015**, *C71*, 3–8.
41. APEX2, Bruker AXS Inc. Madison Wisconsin USA, **2013**.
42. C. F. Macrae, I. J. Bruno, J. A. Chisholm, P. R. Edgington, P. McCabe, E. Pidcock, L. Rodriguez-Monge, R. Taylor, J. van de Streek and P. A. Wood, *J. Appl. Cryst*., **2008**, *41*, 466–470.
43. L. J. Farrugia, *J. Appl. Cryst*., **2012**, *45*, 849–854.